Graefes Arch Clin Exp Ophthalmol (2013) 251:2371–2382
DOI 10.1007/s00417-013-2362-z

GLAUCOMA

The glaucoma detection capability of spectral-domain OCT and GDx-VCC deviation maps in early glaucoma patients with localized visual field defects

Jung Hwa Na · Kyoung Sub Lee · Jong Rak Lee · Youngrok Lee · Michael S. Kook

Received: 13 October 2012 / Revised: 15 April 2013 / Accepted: 22 April 2013 / Published online: 3 July 2013

Abstract
Purpose To evaluate and compare the glaucoma detection capabilities afforded by retinal nerve fiber layer (RNFL) thickness and deviation maps obtained using Cirrus spectral domain optical coherence tomography (Cirrus OCT), and GDx employing variable corneal compensation (GDx-VCC) in glaucoma patients with early, localized visual field (VF) loss.
Methods This prospective controlled, comparative study was performed on 42 eyes with localized VF defects, and 42 age/refractive error-matched healthy eyes. All participants were imaged by both imaging devices at the same visit. The area of the RNFL defect in each deviation map, corresponding to a VF defect, was analyzed by direct counting of color-coded superpixels in each device. Receiver operating characteristic (ROC) curves were constructed and compared between Cirrus OCT and GDx-VCC.
Results The areas under the ROCs (AUCs) of RNFL quadrant thicknesses in hemifields with visual field (VF) defects did not differ significantly (Cirrus OCT; 0.961, GDx-VCC; 0.919, P=0.07). However, Cirrus OCT afforded a better diagnostic ability, by deviation map analysis, than did GDx-VCC (0.972 vs 0.887, P=0.02).
Conclusions The RNFL thicknesses assessed by either Cirrus OCT or GDx-VCC were comparable in terms of early glaucoma diagnostic capability. However, when areas containing RNFL defects were analyzed via deviation mapping, Cirrus OCT was better than GDx-VCC.

Keywords Cirrus spectral-domain optical coherence tomography (SD-OCT) · Deviation map · GDx employing variable corneal compensation (GDx-VCC) · Glaucoma · Retinal nerve fiber layer (RNFL)

The authors have no proprietary interest, and received no financial support in the development or marketing of instruments or pieces of equipment mentioned in this article, nor any competing instrument or equipment.

J. H. Na · K. S. Lee · J. R. Lee · M. S. Kook (✉)
Department of Ophthalmology, University of Ulsan,
College of Medicine, Asan Medical Center,
388-1 Pungnap-2-dong, Songpa-gu,
Seoul, Korea 138-736
e-mail: mskook@amc.seoul.kr

Y. Lee
Gyeonggi Provincial Medical Center, Suwon, Republic of Korea

Introduction

Retinal nerve fiber layer (RNFL) defects are reported to precede development of apparent visual field (VF) abnormalities in some glaucomatous eyes [1, 2]. Thus, detection of localized RNFL defects is critically important if glaucoma is to be diagnosed early. RNFL photography has served as the gold standard for detection of such defects. However, interpretation of RNFL photographs is rather subjective, and does not allow RNFL defects to be quantified in any manner. Therefore, imaging devices providing objective and quantitative information on RNFL assessment have become valuable for structural assessment of the RNFL in glaucoma patients [3, 4]. Both scanning laser polarimetry (SLP) and optical coherence tomography (OCT) are employed to this end.

The SLP (a GDx-VCC instrument; Carl Zeiss Meditec, Inc., Dublin, CA, USA) is an imaging device that estimates RNFL thickness by measuring the summed retardation of a polarized scanning laser beam induced by the microtubule birefringence of retinal ganglion cell (RGC) axons. RNFL assessment by GDx-VCC has been shown to be accurate in many studies [3–5]. For each image, an ellipse or circle was placed

around the inner margin of the sclera ring by one operator. This resulted in a 10-pixel-wide RNFL thickness measurement ellipse of 1.75 times the diameter of the disc in the circumpapillary retina. The ellipse was divided into superior and inferior segments of 120° each, a nasal segment of 70°, and a temporal segment of 50°. Additionally, GDx-VCC yields a deviation map which shows RNFL assessment and statistical deviations from the internal normative database within the circumpapillary area, permitting the pattern and size of RNFL loss around the optic disc to be evaluated. The deviation map is, therefore, similar to the image obtained using red-free photography.

Cirrus spectral-domain optical coherence tomography (Cirrus OCT) (Carl Zeiss Meditec, Inc., Dublin, CA, USA) affords a higher lateral and axial resolution and has a faster scan speed than offered by conventional time-domain (TD) Stratus OCT (Carl Zeiss Meditec). RNFL assessments via Cirrus OCT are highly reproducible, and the sensitivity and specificity of such assessments in terms of glaucoma detection are comparable to, or better than, the values yielded by earlier OCT versions [6–10]. The high scanning speed allows construction of a three-dimensional RNFL thickness deviation map of a 6×6 mm circumpapillary RNFL area. This is an advantage of spectral-domain (SD)-OCT compared to TD-OCT.

Although the two imaging devices, GDx-VCC and Cirrus OCT, provide RNFL assessment in different ways, both devices yield RNFL deviation maps that may facilitate timely detailed recognition of glaucomatous RNFL damage. However, current GDX-VCC and Cirrus OCT deviation maps do not afford quantitative data, but rather yield only patterns and size of RNFL thickness maps with statistical significance in comparison to the built-in normative database. With both Cirrus OCT and GDx-VCC, quantitative data from deviation maps not only facilitates the estimation of the size of deviation map that might be significantly associated with a real presence of glaucoma, but also provides further information with regard to possible progression of the disease, based on the longitudinal change of deviation map in a quantitative manner when glaucoma patients are followed over time.

In the present study, we sought to quantify RNFL changes revealed in Cirrus OCT and GDx-VCC deviation maps, based on superpixel count, and compared the glaucoma diagnostic capabilities afforded by such estimate in early glaucoma patients with localized VF loss, as glaucoma often commences with development of a localized VF defect in one hemifield [1, 2]. To the best of our knowledge, this is the first report to explore and compare the ability of deviation maps developed from two different imaging devices using different RNFL assessment principles to detect glaucoma in patients with localized VF defects.

Materials and methods

Subjects

All study subjects were recruited prospectively, in a consecutive manner, between September 2010 and February 2012, at the Asan Medical Center, Seoul, Korea. At initial evaluation, each patient routinely underwent a complete ophthalmologic examination including the taking of medical, ocular, and family histories, best-corrected visual acuity (BCVA) assessment, slit-lamp biomicroscopy, Goldmann applanation tonometry (GAT), gonioscopy, dilated fundoscopic examination using a 90- or 78-diopter (D) lens, stereoscopic optic disc and RNFL red-free photography (EOS D60 digital camera; Canon, Tochigiken, Japan), a visual field (VF) test using a Humphrey field analyzer (HFA) employing the Swedish Interactive Threshold Algorithm 24–2 (SITA, Carl Zeiss Meditec), axial length measurement using an IOL Master (Carl Zeiss Meditec), central corneal thickness (CCT) measurement employing ultrasound pachymetry (DGH-550; DGH Technology Inc., Exton, PA, USA), circumpapillary RNFL thickness measurement via Cirrus-OCT, and scanning laser polarimetry (GDx-VCC). To minimize any learning effect, the first VF test results were excluded from analysis.

For inclusion in the study, all participants had to meet the following criteria: (1) 18 years of age and older, (2) best-corrected VA of 20/30 or better, with a spherical equivalent within±5 diopter (D) and a cylinder correction within +3 D, (3) presence of a normal anterior chamber and open-angle on slit-lamp and gonioscopic examinations, and (4) reliable HFA test results with a false-positive error <15 %, a false-negative error <15 %, and a fixation loss <20 %. Subjects with evidence of an intracranial or otolaryngeal lesion, with a history of massive hemorrhage or hemodynamic crisis, who presented with any other ophthalmic disease that could result in VF defects, or with a history of diabetes mellitus or eye surgery/laser treatment, were excluded. Central corneal thickness was not a factor in either inclusion or exclusion process.

Glaucoma patients had to meet the following criteria regardless of intraocular pressure (IOP) level since normal-tension glaucoma (NTG) is a relatively common form of glaucoma in our part of the Asia: (1) localized VF loss confined to one side of the horizontal meridian on HFA, confirmed by both examiners (M.S.K. and J.H.N.), (2) glaucomatous VF defined as a glaucoma hemifield test (GHT) result outside normal limits, a pattern standard deviation (PSD) outside 95 % of normal limits, and a cluster of three or more points in the pattern deviation (PD) plot in a single hemifield (superior or inferior) with P values <0.05, one of which had a P value <0.01, and, (3) open anterior chamber angles on slit-lamp biomicroscopy and gonioscopy in both eyes. The definition of a localized hemifield defect required the following characteristics: (1) three or more

adjacent points with $P<0.05$ in a PD probability map, or two or more adjacent points with $P<0.02$ in a superior or inferior hemifield, and, (2) the hemifield of the other side had no clusters of three points with $P<0.05$ and no clusters of two points with $P<0.02$ on either total deviation (TD) or PD probability maps. All findings were confirmed on two consecutive VF examinations in the study group, and the second VF data were used in the final analysis.

A control group consisted of clinic staff, friends or spouses of patients, and volunteers from other specialty clinics. Control group inclusion criteria were IOP <22 mmHg, no history of IOP elevation above 21 mmHg, absence of optic nerve head abnormality, and a normal HFA examination. Normal control subjects were consecutively selected to match glaucoma patients by age (± 5 years) and refractive error (± 2 diopters). Twenty-nine superior hemifields were selected from control group to match the superior hemifield defects ($n=29$) in glaucomatous group, while 13 inferior hemifields to match the inferior hemifield defects ($n=13$) in glaucomatous eyes were selected. The hemiretinas opposite to the selected hemifields ($n=29$, superior hemifields; $n=13$, inferior hemifields) in control eyes served as matching hemiretinas to those hemiretinas opposite to the corresponding hemifield defects in glaucomatous eyes. The matched RNFL areas in control eyes were the hemiretinas opposite to the selected matching hemifields. All participants gave written informed consent before enrollment. All procedures conformed to the Declaration of Helsinki, and the study was approved by the Institutional Review Board of the Asan Medical Center at the University of Ulsan, Seoul, Korea.

GDx with variable corneal compensation (VCC)

The general principles of SLP employing variable corneal polarization compensation have been described in detail elsewhere [11, 12]. After obtaining data using GDx-VCC version 5.6.0.8, information from eyes that yielded scan quality scores of 8 or better was analyzed. All accepted images showed a centered optic disc, were well-focused, were adequately illuminated over the entire image, and did not show motion artifacts. We defined the atypical retardation pattern (ARP) as retardation maps showing alternating circumpapillary circumferential bands of low and high retardation, maps with areas of high retardation that were variable in extent and that were arranged in a spoke-like circumpapillary pattern, and maps showing splotchy areas of high retardation temporally and/or nasally. Current GDx-VCC software provides an exportable parameter called typical scan score (TSS) that provides a numerical score that represents the degree of "typicalness" in each scan, ranging from 1 (extremely atypical) to 100 (very typical). A glaucoma specialist (J.H.N.) first excluded ARP images based on subjective judgement, and then images with TSS less than 80 were further excluded subsequently from the rest of the study group, which was based on the study by Bagga and Greenfield [13]. Therefore, GDx-VCC images that had TSS score ≥80 and without ARP based on subjective inspection by a glaucoma specialist (JHN) were only included in the study in order to remove any effect of ARP on RNFL assessment using GDx-VCC in the current study. The distributions of TSS in normal and glaucoma subjects were from 90 to 100 and from 80 to 100 respectively.

The deviation map output of the GDx-VCC compares patient RNFL thickness values with those in an age-matched normal database, at each superpixel (4×4 pixels). Superpixels are displayed in one of four colors, revealing differences in deviation levels; dark blue (the probability of <5 % that normal subjects of the same age would have the same RNFL thickness), light blue (probability of <2 %), yellow (probability of <1 %), and red (probability of <0.5 %).

Cirrus optical coherence tomography

The basic principles and technical characteristics of SD-OCT have been described elsewhere [8, 14, 15]. All Cirrus OCT scans included in analysis had signal strengths of better than 6, and no motion artifact was evident within the measurement circle of the en-face image. RNFL thickness measurements were obtained from optic disc cube data composed of 200 A-scans derived from 200 B-scans. Abnormal RNFL measurements within the analyzed 6×6 mm cicumpapillary area are displayed in the RNFL thickness deviation map. The map is composed of 50×50 superpixels. A superpixel is colored yellow or red if the RNFL thickness measurement falls below 95 % or 99 %, respectively, of the percentile range.

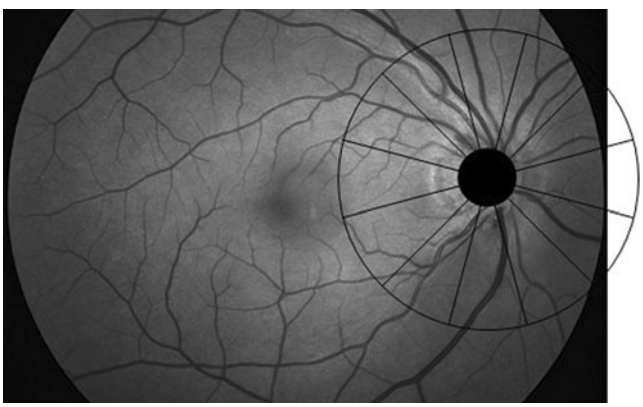

Fig. 1 The determination of clock-hour location of RNFL defect in RNFL red-free photograph. This eye has inferior RNFL defect from 6 to 7 o'clock position in the hemiretina, corresponding with VF scotoma, and also has narrow RNFL defect in the superior hemiretina at the 11 o'clock position, corresponding with inferior normal VF

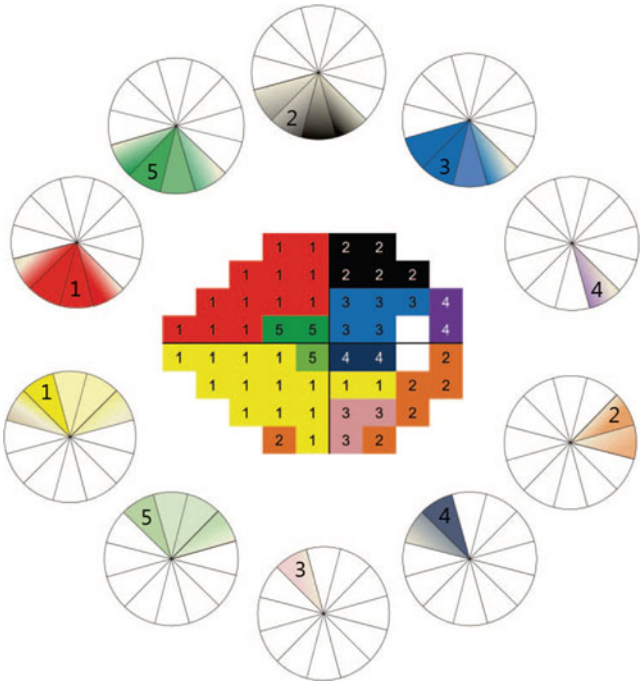

Fig. 2 The relationship between the sectors into which test points of the visual field were divided by the factor analysis, and the RNFL thickness, measured with OCT. The stronger the correlation between structure and function, the sharper the color in the 12 clock hour maps

Evaluation of red-free photography

To determine the direction and range of RNFL defect in RNFL photographs, 12 clock-hours were drawn around the optic disc margins in consecutive photographs (Fig. 1). During this process, the optic disc was manually blackened by a masked observer to avoid bias during assessment of the RNFL defects on red-free photography. If the difference of RNFL position between the photograph and deviation map was within one clock-hour, then we defined that the deviation map coincided with photographs.

RNFL abnormality of deviation map

In the consecutive deviation map printout, we considered that an RNFL abnormality was present when clusters of abnormal pixels originated from the optic disc margin, were wider than one retinal vessel in diameter, and were wedge- or fan-shaped.

Mapping VF to RNFL deviation map

The map of Ferreras et al. (Fig. 2) [16] was used to determine clock-hour RNFL sectors containing localized VF defects. In brief, each hemifield was divided into five VF regions correlating with OCT RNFL thickness clock-hours upon factor analysis. Within a given region of a VF defect in a hemifield, an overlap in the representation of RNFL abnormalities was evident. In fact, there is no one-to-one correspondence between a questioned subfield and a specific portion of circumpapillary RNFL sector, as in the papers by Ferreras et al. [16] and Garway-Heath et al. [17]. Therefore, we calculated all of abnormal pixel counts within the clock-hour regions corresponding to localized VF defects according to the map of Ferreras et al. [16] on the deviation maps obtained using either SLP or Cirrus OCT. Figure 3 shows an eye with superior VF scotoma. We divided the scotoma according to the map of Ferreras et al. [16] into A, B, and C zone. Each zone is correlated with RNFL thickness from 5 to 8 o'clock positions according to the map of Ferreras et al. [16]. On the deviation maps, abnormal pixel counts that originated from the optic disc margin, were wider than one retinal vessel in diameter, and were wedge- or fan-shaped between 5 and 8 o'clock positions, were performed. In this eye, definite RNFL abnormalities were detected from 6 to 7 o'clock positions, and we

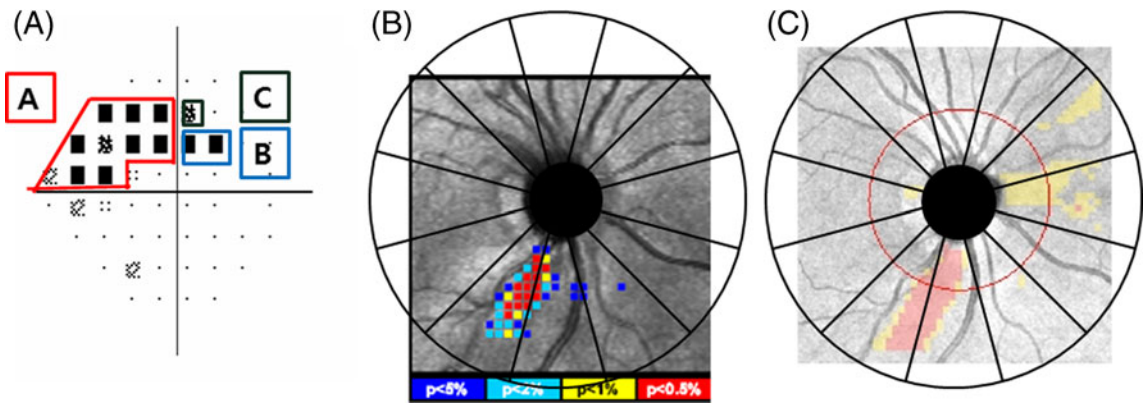

Fig. 3 Glaucoma in the right eye. **a** The Humphrey field analyzer printout reveals superior visual field defects on the pattern deviation map, in zones (*A*=1, *B*=3, and *C*=2) as classified by Ferreras et al. The corresponding areas in the circumpapillary retina are the 5, 6, 7, and 8 o'clock positions. **b** The numbers of superpixels were counted in corresponding area (from 5 to 8 o'clock positions) of GDx-VCC deviation map. **c** The number of superpixels were counted in the corresponding area (from 5 to 8 o'clock positions) of Cirrus OCT deviation map

Table 1 Demographics of the glaucoma and control groups (means ± standard deviations)

		Glaucoma	Control	*P*-value
N		42	42	
Eyes (OD/OS)		20/22	24/18	0.382*
Gender (M/F)		21/21	19/23	0.662*
Age (years)		50.69±10.34	50.76±9.77	0.946†
Visual acuity (VA, decimal)		0.90±0.15	0.96±0.21	0.266†
Spherical equivalent (SE, diopters)		−1.25±1.75	−1.11±1.79	0.571†
Axial length (mm)		23.7±1.0	23.5±1.1	0.511†
Intraocular pressure (IOP, mmHg)		15.43±2.49	14.24±2.85	0.058†
Central corneal thickness (μm)		535.3±37.5	543.7±36.9	0.045†
Vertical cup-to-disc ratio (stereo optic nerve photography by a glaucoma expert)		0.73±0.14	0.55±0.12	<0.001†
Mean deviation (MD, dB)		−4.19±2.06	−0.84±1.49	<0.001†
Pattern standard deviation (PSD)		6.04±3.45	1.56±0.35	<0.001†
Hemifield with VF loss (superior/inferior)		29/13	NA	
OCT RNFL thickness map	Average (μm)	76.79±9.09	96.67±9.07	<0.001†
	Superior quadrant (μm)	98.62±20.75	121.62±20.88	<0.001†
	Inferior quadrant (μm)	85.62±23.47	124.05±14.73	<0.001†
GDx TSNIT parameters	Average (μm)	46.97±5.50	58.31±5.65	<0.001†
	Superior average (μm)	57.77±11.39	72.07±7.43	<0.001†
	Inferior average (μm)	50.62±9.42	66.93±10.86	<0.001†
GDx NFI		37.45±15.54	14.10±7.82	NA

NA not applicable

*chi-squared test

† independent samples *t*-test

performed the abnormal pixel counts in these clock-hour positions (Fig. 3). To determine the clock-hour location of the optic disc in the deviation map, 12 clock-hours were drawn around the optic disc margins shown in consecutive deviation maps. During this process, the optic disc was manually blackened by a masked observer to avoid bias during assessment of the RNFL defects on deviation maps (Fig. 3).

In each deviation map yielded by GDx-VCC, the numbers of abnormal superpixels at each probability level (dark blue $P<0.05$, light blue $P<0.02$, yellow $P<0.01$, or red $P<0.005$) in clock-hour areas corresponding to VF defects were counted. When the normative deviation map abnormality was defined as less than 5 %, four types of abnormal superpixels were counted; when the deviation map

Table 2 Comparisons of abnormal retinal nerve fiber layer (RNFL) thickness and superpixel count from the retinal regions corresponding to hemifields, showing visual field loss (means ± standard deviations, with ranges)

		Glaucoma	Control	*P*-value*
Cirrus OCT parameters				
RNFL thickness map	Quadrant thickness corresponding to hemifields VF defects (μm)	78.95±20.13	124.90±15.14	<0.001
RNFL deviation map	Abnormal pixel count ($P<5$ %)			<0.001
	Abnormal pixel count ($P<1$ %)			<0.001
GDx VCC parameters				
TSNIT parameters	Quadrant thickness corresponding to hemifields VF defects (μm)	49.00±10.29	68.10±11.13	<0.001
RNFL deviation map	Abnormal superpixel count ($P<5$ %)	47.69±44.42 (0.00–169.00)	2.36±7.89 (0.00–33.00)	<0.001
	Abnormal superpixel count ($P<1$ %)	19.88±23.77 (0.00–84)	0.33±1.57 (0.00–9.00)	<0.001

VF visual field

*independent samples *t*-test

Table 3 Likelihood ratios of deviation maps yielded by Cirrus OCT and GDx-VCC

	Cirrus OCT		GDx-VCC	
	Glaucoma	Control	Glaucoma	Control
Detection of an RNFL defect (*n*)	41	3	35	4
No detection of an RNFL defect (*n*)	1	39	7	38
Sensitivity (95 % CI*)	0.976 (0.859–0.999)		0.833 (0.680–0.925)	
Specificity (95 % CI*)	0.929 (0.794–0.981)		0.905 (0.765–0.969)	
(+) LR (95 % CI*)	13.667 (4.588–40.707)		8.750 (3.411–22.443)	
(−) LR (95 % CI*)	0.030 (0.004–0.178)		0.184 (0.093–0.364)	

LR likelihood ratio,**CI* confidence interval

abnormality was defined as less than 1 %, yellow and red superpixels were counted.

In each deviation map yielded by Cirrus OCT (running software version 3.0), the size of RNFL defect was identified as the number of superpixels coded in red ($P<0.01$) and yellow ($P<0.05$). As the software used in the current study did not provide automatic measurement of the size of RNFL defects in superpixels, a computer program was written in Mathlab R2007a (The MathWorks, Inc., Natick, MA, USA) to analyze the size of RNFL defects in superpixels based on the Cirrus OCT deviation map [18]. We counted red ($P<1$ %) or yellow and red ($P<5$ %) superpixels in areas of abnormal RNFL thickness in each deviation map, which were matched to regions in the opposite hemifield that contained localized VF defects after optic disc margin was outlined in the exported RNFL thickness deviation map (Fig. 3). Areas of abnormal superpixels that were amorphous in shape, nasally located, or that presented as islands in regions remote from the optic disc margin, were excluded.

Statistical analysis

For comparison of RNFL assessment in terms of glaucoma detection between Cirrus OCT and GDx-VCC, superior or inferior quadrant thicknesses were selected depending on the location of VF loss, since the minimal area of RNFL assessment provided by GDx-VCC is quadrant thickness. In other words, if an eye had a VF defect in the superior hemifield, the inferior quadrant RNFL thickness values as determined by both Cirrus OCT and GDx-VCC were analyzed. The independent samples *t*-test was used to compare means between the two groups (glaucoma vs normal). Categorical variables were analyzed using the chi-squared test.

The agreement between the RNFL red-free photographs and deviation maps of Cirrus OCT and GDx-VCC with respect to RNFL defect location was calculated using Kappa analysis. A Kappa value 0.00–0.20 indicates slight agreement, a value 0.21–0.40 fair agreement, a value 0.41–0.60 moderate agreement, a value 0.61–0.80 substantial agreement, and a value 0.81–1.00 almost perfect agreement [19].

Receiver operating characteristic (ROC) curves were constructed to test the ability of RNFL thickness data, abnormal RNFL thickness superpixel counts from GDx-VCC and Cirrus OCT deviation maps, and nerve fiber indicator (NFI) from GDx-VCC, to differentiate glaucomatous eyes with localized VF defects from healthy eyes. Between-instrument AUCs were compared, and the DeLong method was used to evaluate statistical differences between the AUCs yielded by the two devices. Positive and negative likelihood ratios (LRs) for abnormal RNFL change detection using deviation maps showing VF defects were calculated for each device; 95 % confidence intervals (CIs) for each LR were also obtained.

Correlations between RNFL abnormality parameters (RNFL thicknesses and abnormal RNFL superpixel counts in deviation maps showing VF loss), on the one hand, and VF sensitivities, on the other, were investigated using linear regression. VF sensitivity was calculated as the average value of each test point in the abnormal hemifield showing localized scotoma in either the total deviation map (TD) or pattern deviation map (PD).

All statistical analysis was performed using SPSS version 15.0 (SPSS Inc., Chicago, IL, USA) or MedCalc version 11.3.6.0 (MedCalc, Mariakerke, Belgium).

Results

Four eyes were excluded due to having TSS <80 and atypical image judged by a glaucoma expert (J.H.N.), and two eyes were further excluded due to atypical image judged by a glaucoma expert despite having TSS score of 90 in the glaucoma patients. No subject was excluded in the control group based on either TSS score or subjective assessment. After exclusion of images with ARPs (six eyes) and those of poor quality (three eyes), the final sample included data from 84 eyes of 84 subjects (42 patients with glaucoma and 42 normal controls).

The baseline demographic characteristics of the two groups are summarized in Table 1. Both Cirrus OCT and GDx-VCC RNFL thickness measurements (including the average values, the superior quadrant averages, and the

Table 4 Areas under receiver operating characteristic curves (AUCs)

	AUC (95 % CI*)		P**		P***	Sensitivity (specificity)			
						At specificity 85 %		At specificity 95 %	
	OCT	GDx-VCC	OCT	GDx- VCC		OCT	GDx- VCC	OCT	GDx- VCC
Average thickness	0.944 (0.871–0.982)	0.933 (0.857–0.976)	0.81	0.09	0.64	90.48 (85.71)	90.48 (88.10)	71.43 (95.24)	73.81 (95.24)
Quadrant thickness	0.961 (0.895–0.991)	0.919 (0.839–0.967)	0.67	0.07	0.08	90.48 (88.10)	83.33 (88.10)	85.71 (95.24)	71.43 (95.24)
Abnormal pixel count (P<5 %)	0.972 (0.910–0.996)	0.887 (0.800–0.946)			0.02	97.62 (92.86)	83.33 (90.48)	88.10 (97.62)	61.90 (95.24)
Abnormal pixel count (P<1 %)	0.970 (0.908–0.995)	0.855 (0.762–0.923)			0.01	95.24 (92.86)	73.81 (95.24)	92.86 (97.62)	73.81 (95.24)

*CI Confidence interval,

**Comparisons of ROC curves yielded by thickness values and abnormal pixel count (P<5 %), using the DeLong method

***Comparisons of ROC curves yielded by Cirrus OCT and GDx-VCC using the DeLong method

inferior quadrant averages) differed significantly between glaucomatous and normal control eyes.

RNFL quadrant average thickness measurements, and abnormal superpixel counts in the retinal area corresponding to the hemifield showing visual loss, differed between glaucomatous and normal subjects (Table 2).

The Kappa values between RNFL red-free photographs and Cirrus OCT deviation maps and GDx-VCC deviation maps in the hemiretina corresponding with VF scotoma were 0.88 (SE=0.05, P<0.01), and 0.74 (SE=0.07, P<0.01) respectively. The Kappa values between RNFL red-free photographs and Cirrus OCT deviation maps and GDx-VCC deviation maps in the hemiretina corresponding with normal hemifield were 0.44 (SE=0.10, P<0.01), and 0.32 (SE=0.11, P<0.01) respectively.

The Cirrus OCT deviation maps of areas showing localized hemifield VF defects afforded higher sensitivity and specificity than did GDx-VCC deviation maps in terms of detection of an abnormal RNFL (Table 3). LRs calculated following Jaeschke et al. [20] were associated with large and moderate effects, respectively, on post-test Cirrus OCT and GDx-VCC probabilities.

Average RNFL thickness measurements obtained using either Cirrus OCT or GDx-VCC afforded good glaucoma discrimination capabilities; no significant difference was evident between the two instruments (AUC 0.944 vs 0.933; P= 0.64). The RNFL thickness in the quadrant showing VF loss did not differ significantly when Cirrus OCT and GDx-VCC data were compared. The glaucoma diagnostic capabilities thus afforded were similar (AUC 0.961 vs 0.919; P=0.08). However, the counting of abnormal superpixels on the deviation map of the region showing VF loss revealed that Cirrus OCT could detect glaucomatous defects better than could GDx-VCC. The glaucoma diagnostic capabilities of average and quadrant thicknesses showing VF loss did not differ statistically from those of abnormal pixel counts (P<5 %) in a given device (Cirrus OCT; P=0.81, 0.67; GDx-VCC; P= 0.09, 0.07 respectively) (Table 4). The glaucoma diagnostic capability of GDx-VCC NFI did not differ statistically from those of abnormal pixel counts (P<5 %) (Cirrus OCT; P= 0.18, GDx-VCC; P=0.21 respectively) and average thickness in a given device (Cirrus OCT; 0.68, GDx-VCC; P=0.93 respectively) (Table 5). Figure 4 (a) and (b) shows AUC curves describing the diagnostic accuracy for RNFL thickness, abnormal pixel counts from Cirrus OCT and GDx-VCC, and GDx-VCC NFI.

Table 6 shows the correlations between Cirrus OCT and GDx-VCC parameters, on the one hand, and the VF sensitivities in the abnormal hemifield corresponding to localized scotoma, on the other, using both TD and PD. Not surprisingly, in quadrants showing VF loss, not only RNFL thicknesses, but also the counts of abnormal superpixels on deviation maps, correlated significantly with the relevant

Table 5 Areas under receiver operating characteristic curves (AUCs) of GDx-VCC

	AUC (95 % CI*)	P**	P***	P****	P*****
GDx-VCC NFI	0.932 (0.856–0.976)	0.18	0.21	0.68	0.93

**CI* confidence interval,

**Comparisons of ROC curves yielded by NFI and OCT abnormal pixel count ($P<5$ %), using the DeLong method

***Comparisons of ROC curves yielded by NFI and GDx-VCC abnormal pixel count ($P<5$ %), using the DeLong method

****Comparisons of ROC curves yielded by NFI and OCT average thickness, using the DeLong method

*****Comparisons of ROC curves yielded by NFI and GDx-VCC average thickness, using the DeLong method

average TD and PD values of affected hemifields, when either Cirrus OCT or GDx-VCC data were evaluated.

Discussion

Localized VF defects are often associated with localized RNFL defects [1, 2, 21]. The present study is unique in that we sought to analyze and compare quantitative data yielded by deviation maps constructed by both GDx- VCC and Cirrus OCT from eyes with localized glaucomatous VF defects. Previously, Lee et al. [22] compared the glaucomatous diagnostic ability of GDx VCC and Cirrus OCT measurements. They analyzed only thickness parameters, not deviation maps. They reported that both Cirrus OCT and GDx-VCC RNFL thicknesses showed good glaucoma diagnostic capabilities, but Cirrus OCT showed higher sensitivities than GDx-VCC in detecting glaucomatous eyes with early to moderate VF defects (MD=−6.33 dB). In the current study, the subjects with early glaucoma were targeted. At the early stage of glaucoma, the RNFL thickness measured by Cirrus OCT and GDx-VCC showed comparable diagnostic ability, but, when RNFL defects were analyzed via deviation mapping, Cirrus OCT was better than GDx-VCC in terms of glaucoma detection.

In an RNFL deviation map, circumpapillary RNFL measurements that are below the 95 % value of the normal percentile range are color-coded; this allows the location and distribution pattern of circumpapillary RNFL abnormalities to be ascertained at a glance in clinical situations. Recently, Ye et al. [23] reported that an SD-OCT deviation map revealed RNFL abnormalities that were not detectable by confocal scanning laser ophthalmoscopy, and the cited authors suggested that a deviation map may be superior to conventional RNFL photography in terms of detection of RNFL changes in glaucoma.

Previously, Kook et al. [5] developed an algorithm to analyze data from GDx-VCC deviation maps, and suggested that use of their approach might aid in the understanding of GDx-VCC data in terms of localization, deviation size, and severity of localized RNFL defects in eyes with localized VF loss. Not only data obtained using the algorithm, but also the simple superpixel numbers yielded by analysis of GDx-VCC deviation maps, correlated significantly with VF indices. More recently, Leung et al. [14] developed a scoring system for analysis of Cirrus OCT deviation map abnormalities, and found that deviation maps yielding high scores afforded excellent sensitivity in terms of glaucoma detection. In addition, Kang et al. [24] constructed an algorithm that was used to analyze Cirrus OCT deviation maps; the procedure detected localized VF defects more reliably than did circular RNFL thickness scan around the optic nerve head. Therefore, these studies indicate that deviation maps from these imaging devices with different working principles might provide better glaucoma detection capabilities than circumpapillary RNFL thickness measurement. However, there have been no reports addressing and comparing the diagnostic performance of deviation maps of Cirrus OCT and GDx-VCC from the same cohort group.

With this in mind, we sought to compare the glaucoma detection capabilities of deviation maps yielded by GDx-VCC and Cirrus OCT from the same cohort of early glaucomatous subjects. Although both instruments provide RNFL assessment using deviation maps, neither supplies quantitative data based on such maps. Thus, to quantify abnormalities revealed by such maps, we counted the numbers of abnormal superpixels ($P<5$ % and <1 %) on both GDx-VCC and Cirrus OCT deviation maps.

When we examined abnormal RNFL thickness data in the regions of the deviation maps that were associated with localized VF loss, we found that Cirrus OCT afforded better sensitivity and specificity than did GDx-VCC (sensitivity and specificity 0.976 and 0.929 vs 0.833 and 0.905 respectively) (Table 3). In addition, superpixel counts also revealed the superior diagnostic capability of Cirrus OCT compared to GDx-VCC (at the 5 % level: 0.972 vs 0. 887, $P=0.02$; at the 1 % level: 0.970 vs 0.855, $P=0.01$) (Table 4).

One explanation for the fact that Cirrus OCT afforded better glaucoma diagnostic capability than GDx-VCC in our series is that the two devices employ totally different technologies to perform RNFL assessment. Wang et al. [25] have suggested that the difference in the diagnostic abilities of the two instruments may be explained by the distinct

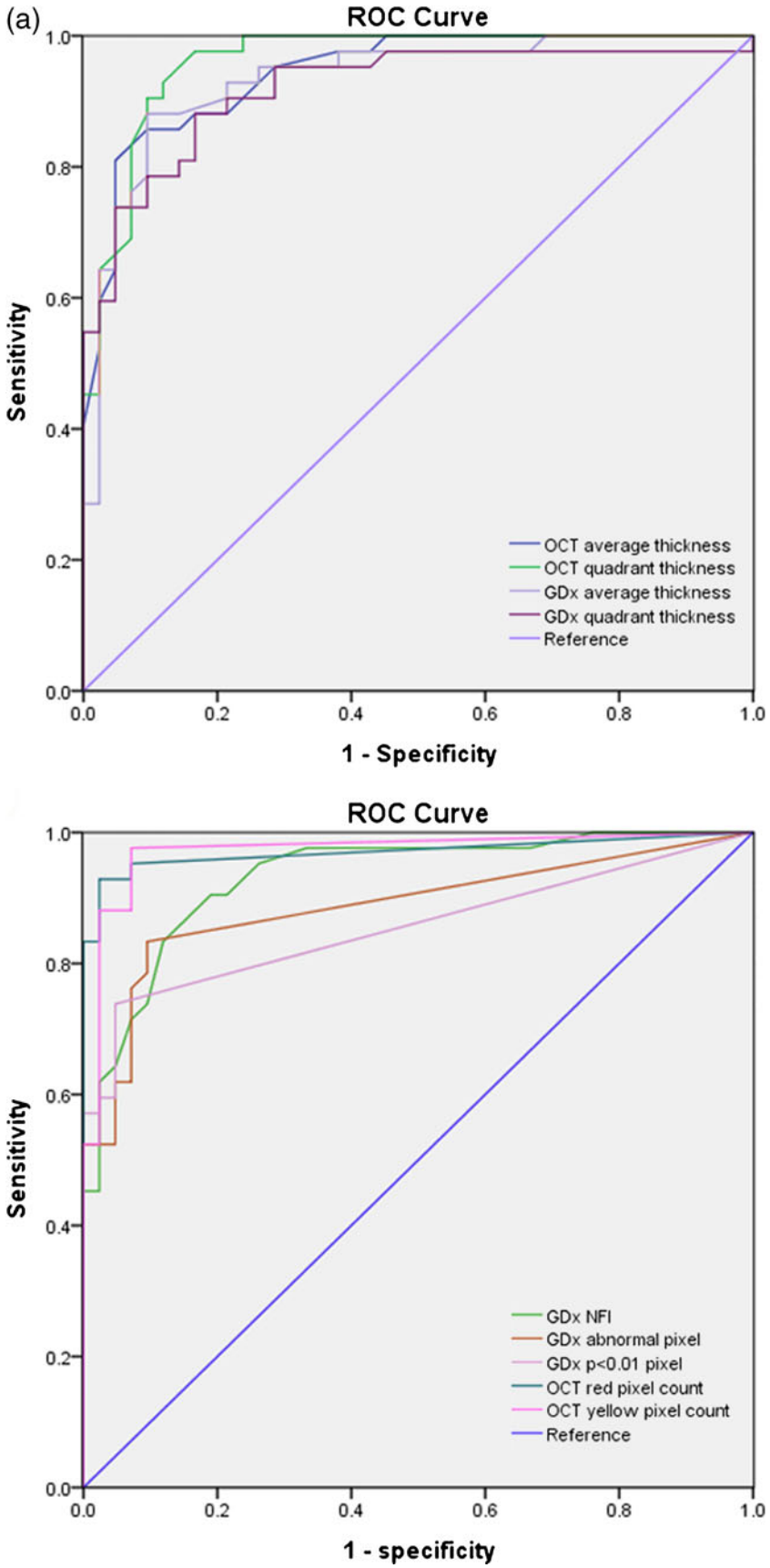

Fig. 4 Areas under receiver operating characteristic curves (AUCs) of Cirrus OCT and GDx-VCC

Table 6 Correlation between abnormal retinal nerve fiber layer (RNFL) thickness and superpixel count yielded by the two imaging devices, and the visual field sensitivities of the corresponding abnormal hemifields

Parameter			vs TD		vs PD	
			R^2	*P*-value*	R^2	*P*-value*
Cirrus OCT	RNFL thickness map	Quadrant thickness corresponding to hemifields VF defects (μm)	0.546	<0.001	0.522	<0.001
	RNFL deviation map	Abnormal pixel count (P<5 %)	0.509	<0.001	0.481	<0.001
		Abnormal pixel count (P<1 %)	0.540	<0.001	0.515	<0.001
GDx- VCC	TSNIT parameter	Quadrant thickness corresponding to hemifields VF defects (μm)	0.300	<0.001	0.303	<0.001
	RNFL deviation map	Abnormal superpixel count (P<5 %)	0.264	<0.001	0.254	<0.001
		Abnormal superpixel count (P<1 %)	0.258	<0.001	0.253	<0.001

VF visual field, *PD* average pattern deviation in the abnormal hemifield, *TD* average total deviation in the abnormal hemifield

*Linear regression analysis

mechanisms used to calculate RNFL thickness. Unlike TD-OCT, in SD-OCT the echo time-delay mode of the TD-OCT is replaced by simultaneous detection of frequency changes. All frequency components are detected using a charge-coupled device. Depth information on the retinal layer, yielded by each frequency component, is obtained after Fourier transformation of each signal [26]. Therefore, theoretically, SD-OCT could reduce inaccurate and unreliable data acquisition which might be originated from improper scanning circle placement or involuntary ocular movement during scanning. GDx-VCC does not measure the actual thickness of the retina but rather birefringence of the RNFL; retinal thickness is calculated using a formula that considers phase retardation and the birefringence constant [25, 27].

GDx-VCC is inadequate to deal with residual anterior segment retardation. In recent studies investigating the effect of ARP, Bagga et al. demonstrated a decreased association between average RNFL measurements obtained with GDx-VCC and those obtained using TD-OCT for atypical scans compared with typical scans [28]. Da Pozzo et al. reported AUC curves for discriminating between healthy eyes and glaucomatous eyes with TSS ≥70 and glaucomatous eyes with TSS <70, and found a significantly higher discriminating ability with GDx-VCC in the glaucomatous eyes with TSS ≥70 than those with TSS <70, indicating that the diagnostic accuracy of GDx-VCC parameters is affected by the presence of atypical retardation patterns [29, 30]. More recently, Hoesl et al. investigated the impact of TSS on discriminating glaucomatous and healthy eyes by GDx-VCC and Spectralis SD-OCT, and found that decreasing TSS was associated with a decrease in diagnostic accuracy for discriminating healthy and glaucomatous eyes by GDx-VCC, while diagnostic accuracy was comparable for SD-OCT and GDx-VCC if typical scans (TSS=100) were investigated [31]. A recently introduced form of GDx, featuring enhanced corneal compensation (ECC), neutralizes uncompensated corneal retardation [32], reduces the influence of atypical retardation signals on RNFL assessments, and increases diagnostic sensitivity [33–36].

Another possible explanation of the differences in the diagnostic capabilities of the two devices may be variation between the internal normative databases of the instruments. Although detailed data are lacking, the subjects analyzed to construct the GDx-VCC normative database include a relatively small proportion of Asians [37], whereas more than 20 % of subjects were Asian when data were gathered for the Cirrus OCT normative database [38]. The greater proportion of Asian ethnic data in the Cirrus OCT database may afford better OCT glaucoma diagnostic accuracy in Asian individuals.

In our series, the deviation map algorithm from Cirrus OCT was slightly more effective than circumpapillary RNFL thickness measurement in discriminating early glaucomatous eyes from those of normal controls. The explanation for this finding is that Cirrus OCT uses a clock-hour or quadrant as the basic unit of calculation and, for calculation of average circumpapillary RNFL thickness in a given participant, RNFL thicknesses from multiple clock-hours corresponding to localized VF defect were averaged and used based on the approach of Ferreras et al. [16]. This may have contributed to a lower sensitivity to detect narrow RNFL defects based on circumpapillary RNFL thickness measurement. Another explanation is that glaucomatous eyes with very early localized VF defect did not show abnormal averaged RNFL thickness values in the quadrant location, while they manifested into abnormal changes in the deviation maps.

The parameters measured by both Cirrus OCT and GDx-VCC correlated significantly with VF sensitivities. Although the AUCs of GDx-VCC parameters were statistically lower than those of Cirrus OCT parameters derived from deviation maps, the AUC values yielded by GDx-VCC were

nonetheless relatively high (0.855–0.919), reflecting good detection of glaucomatous damage. Thus, the observed differences may not be very significant in clinical practice.

The present study had several limitations, including the use of only Asian subjects. It may be inappropriate to make statistical comparisons of an Asian population with normative RNFL data derived from multiple races. Also, we cannot exclude a possible selection bias, in that most of our glaucomatous patients had normal-tension glaucoma; the IOP was below 22 mmHg in most patients (31 of 42; 73.8 %). We counted only abnormal superpixels connected to the optic disc margin that were wider than one vessel in diameter, and that were wedge- or fan-shaped. The results might have been different had we used more lenient criteria for evaluation of RNFL defects in deviation maps. Another limitation is associated with our recruitment method. In the current study, patients with VF loss localized to a single hemifield were included, regardless of the nature of the RNFL defect. In general, RNFL loss precedes VF loss. Therefore, use of RNFL loss revealed by thickness measurement or by deviation mapping of the relevant retina to diagnose glaucoma might have inflated the diagnostic capability of either device. In addition, it is possible, in some eyes, that RNFL loss may not occur in retinal areas showing VF loss. This would cause the diagnostic ability of either device to be underestimated. Finally, only good quality scans with signal strengths greater than 6 with Cirrus OCT, and scan quality scores of 8 or better and TSS score ≥80 with GDx-VCC, were included in the analyses. Caution should be taken when diagnosing glaucoma with a mixture of both good and poor quality scans.

In conclusion, we have shown that use of a Cirrus OCT deviation map was superior to employment of a GDx-VCC deviation map in terms of detection of early glaucomatous eyes. Further, we found that abnormal superpixel counts from Cirrus OCT RNFL deviation maps were associated with somewhat higher AUC values than were RNFL thickness parameters, although the differences were not statistically significant. Quantitative data on abnormal RNFL areas revealed by Cirrus OCT or GDx-VCC deviation mapping may assist in the diagnosis and monitoring of early-stage glaucoma.

References

1. Quigley HA, Katz J, Derick RJ, Gilbert D, Sommer A (1992) An evaluation of optic disc and nerve fiber layer examinations in monitoring progression of early glaucoma damage. Ophthalmology 99:19–28
2. Sommer A, Katz J, Quigley HA, Miller NR, Robin AL, Richter RC, Witt KA (1991) Clinically detectable nerve fiber atrophy precedes the onset of glaucomatous field loss. Arch Ophthalmol 109:77–83
3. Medeiros FA, Zangwill LM, Bowd C, Mohammadi K, Weinreb RN (2004) Comparison of scanning laser polarimetry using variable corneal compensation and retinal nerve fiber layer photography for detection of glaucoma. Arch Ophthalmol 122:698–704
4. Zangwill LM, Bowd C, Berry CC, Williams J, Blumenthal EZ, Sanchez-Galeana CA, Vasile C, Weinreb RN (2001) Discriminating between normal and glaucomatous eyes using the Heidelberg retina tomograph, GDx nerve fiber analyzer, and optical coherence tomograph. Arch Ophthalmol 119:985–993
5. Kook MS, Cho HS, Seong M, Choi J (2005) Scanning laser polarimetry using variable corneal compensation in the detection of glaucoma with localized visual field defects. Ophthalmology 112:1970–1978
6. Vizzeri G, Weinreb RN, Gonzalez-Garcia AO, Bowd C, Medeiros FA, Sample PA, Zangwill LM (2009) Agreement between spectral-domain and time-domain OCT for measuring RNFL thickness. Br J Ophthalmol 93:775–781
7. Sung KR, Kim DY, Park SB, Kook MS (2009) Comparison of retinal nerve fiber layer thickness measured by Cirrus HD and Stratus optical coherence tomography. Ophthalmology 116:1264–1270
8. Park SB, Sung KR, Kang SY, Kim KR, Kook MS (2009) Comparison of glaucoma diagnostic capabilities of Cirrus HD and Stratus optical coherence tomography. Arch Ophthalmol 127:1603–1609
9. Leung CK, Cheung CY, Weinreb RN, Qiu Q, Liu S, Li H, Xu G, Fan N, Huang L, Pang CP, Lam DS (2009) Retinal nerve fiber layer imaging with spectral-domain optical coherence tomography: a variability and diagnostic performance study. Ophthalmology 116:1257–1263, 1263
10. Jeoung JW, Park KH (2010) Comparison of cirrus OCT and stratus OCT on the ability to detect localized retinal nerve fiber layer defects in preperimetric glaucoma. Invest Ophthalmol Vis Sci 51:938–945
11. Zhou Q, Weinreb RN (2002) Individualized compensation of anterior segment birefringence during scanning laser polarimetry. Invest Ophthalmol Vis Sci 43:2221–2228
12. Weinreb RN, Bowd C, Zangwill LM (2003) Glaucoma detection using scanning laser polarimetry with variable corneal polarization compensation. Arch Ophthalmol 121:218–224
13. Bagga H, Greenfield DS (2004) Quantitative assessment of structural damage in eyes with localized visual field abnormalities. Am J Ophthalmol 137:797–805
14. Leung CK, Lam S, Weinreb RN, Liu S, Ye C, Liu L, He J, Lai GW, Li T, Lam DS (2010) Retinal nerve fiber layer imaging with spectral-domain optical coherence tomography: analysis of the retinal nerve fiber layer map for glaucoma detection. Ophthalmology 117:1684–1691
15. Paunescu LA, Schuman JS, Price LL, Stark PC, Beaton S, Ishikawa H, Wollstein G, Fujimoto JG (2004) Reproducibility of nerve fiber thickness, macular thickness, and optic nerve head measurements using Stratus OCT. Invest Ophthalmol Vis Sci 45:1716–1724
16. Ferreras A, Pablo LE, Garway-Heath DF, Fogagnolo P, Garcia-Feijoo J (2008) Mapping standard automated perimetry to the peripapillary retinal nerve fiber layer in glaucoma. Invest Ophthalmol Vis Sci 49:3018–3025
17. Garway-Heath DF, Poinoosawmy D, Fitzke FW, Hitchings RA (2000) Mapping the visual field to the optic disc in normal tension glaucoma eyes. Ophthalmology 107:1809–1815
18. Leung CK, Choi N, Weinreb RN, Liu S, Ye C, Liu L, Lai GW, Lau J, Lam DS (2010) Retinal nerve fiber layer imaging with spectral-domain optical coherence tomography: pattern of RNFL defects in glaucoma. Ophthalmology 117:2337–2344
19. Landis JR, Koch GG (1977) The measurement of observer agreement for categorical data. Biometrics 33:159–174
20. Jaeschke R, Guyatt GH, Sackett DL (1994) Users' guides to the medical literature. III. How to use an article about a diagnostic test. B. What are the results and will they help me in caring for my

patients? The Evidence-Based Medicine Working Group. JAMA 271:703–707
21. Horn FK, Jonas JB, Martus P, Mardin CY, Budde WM (1999) Polarimetric measurement of retinal nerve fiber layer thickness in glaucoma diagnosis. J Glaucoma 8:353–362
22. Lee S, Sung KR, Cho JW, Cheon MH, Kang SY, Kook MS (2010) Spectral-domain optical coherence tomography and scanning laser polarimetry in glaucoma diagnosis. Jpn J Ophthalmol 54:544–549
23. Ye C, To E, Weinreb RN, Yu M, Liu S, Lam DS, Leung CK (2011) Comparison of retinal nerve fiber layer imaging by spectral-domain optical coherence tomography and scanning laser ophthalmoscopy. Ophthalmology 118:2196–2202
24. Kang SY, Sung KR, Na JH, Choi EH, Cho JW, Cheon MH, Kim KH, Kook MS (2012) Comparison between deviation map algorithm and peripapillary retinal nerve fiber layer measurements using Cirrus HD-OCT in the detection of localized glaucomatous visual field defects. J Glaucoma 21:372–378
25. Wang G, Qiu KL, Lu XH, Sun LX, Liao XJ, Chen HL, Zhang MZ (2011) The effect of myopia on retinal nerve fibre layer measurement: a comparative study of spectral-domain optical coherence tomography and scanning laser polarimetry. Br J Ophthalmol 95:255–260
26. Sung KR, Kim JS, Wollstein G, Folio L, Kook MS, Schuman JS (2011) Imaging of the retinal nerve fibre layer with spectral-domain optical coherence tomography for glaucoma diagnosis. Br J Ophthalmol 95:909–914
27. Weinreb RN, Dreher AW, Coleman A, Quigley H, Shaw B, Reiter K (1990) Histopathologic validation of Fourier-ellipsometry measurements of retinal nerve fiber layer thickness. Arch Ophthalmol 108:557–560
28. Bagga H, Greenfield DS, Feuer WJ (2005) Quantitative assessment of atypical birefringence images using scanning laser polarimetry with variable corneal compensation. Am J Ophthalmol 139:437–446
29. Da Pozzo S, Marchesan R, Canziani T, Vattovani O, Ravalico G (2006) Atypical pattern of retardation on GDx-VCC and its effect on retinal nerve fibre layer evaluation in glaucomatous eyes. Eye (Lond) 20:769–775
30. Bowd C, Medeiros FA, Weinreb RN, Zangwill LM (2007) The effect of atypical birefringence patterns on glaucoma detection using scanning laser polarimetry with variable corneal compensation. Invest Ophthalmol Vis Sci 48:223–227
31. Hoesl LM, Tornow RP, Schrems WA, Horn FK, Mardin CY, Kruse FE, Juenemann AG, Laemmer R (2013) Glaucoma diagnostic performance of GDxVCC and spectralis OCT on eyes with atypical retardation pattern. J Glaucoma 22:317–324
32. Toth M, Hollo G (2006) Evaluation of enhanced corneal compensation in scanning laser polarimetry: comparison with variable corneal compensation on human eyes undergoing LASIK. J Glaucoma 15:53–59
33. Toth M, Hollo G (2005) Enhanced corneal compensation for scanning laser polarimetry on eyes with atypical polarisation pattern. Br J Ophthalmol 89:1139–1142
34. Mai TA, Reus NJ, Lemij HG (2007) Diagnostic accuracy of scanning laser polarimetry with enhanced versus variable corneal compensation. Ophthalmology 114:1988–1993
35. Medeiros FA, Bowd C, Zangwill LM, Patel C, Weinreb RN (2007) Detection of glaucoma using scanning laser polarimetry with enhanced corneal compensation. Invest Ophthalmol Vis Sci 48:3146–3153
36. Reus NJ, Zhou Q, Lemij HG (2006) Enhanced imaging algorithm for scanning laser polarimetry with variable corneal compensation. Invest Ophthalmol Vis Sci 47:3870–3877
37. Choi J, Cho HS, Lee CH, Kook MS (2006) Scanning laser polarimetry with variable corneal compensation in the area of apparently normal hemifield in eyes with normal-tension glaucoma. Ophthalmology 113:1954–1960
38. Mwanza JC, Durbin MK, Budenz DL, Girkin CA, Leung CK, Liebmann JM, Peace JH, Werner JS, Wollstein G (2011) Profile and predictors of normal ganglion cell-inner plexiform layer thickness measured with frequency-domain optical coherence tomography. Invest Ophthalmol Vis Sci 52:7872–7879